ERNEST ORLANDO LAWRENCE BERKELEY NATIONAL LABORATORY

BERKELEY LAB

Detector Implications for Electroweak Physics at the Tevatron

Ronald J. Madaras
Physics Division

MASTER

DISCLAIMER

Detector Implications for Electroweak Physics at the Tevatron *

Ronald J. Madaras

PHYSICS DIVISION
Lawrence Berkeley National Laboratory,
Berkeley, California 94720

December 1996

DISCLAIMER

Portions of this document may be illegible in electronic image products. Images are produced from the best available original document.

Detector Implications for Electroweak Physics at the Tevatron *

Ronald J. Madaras[a]

[a]Lawrence Berkeley National Laboratory,
University of California, Berkeley, CA, USA 94720

· This paper discusses how various performance aspects of the DØ and CDF detectors at the Fermilab Tevatron Collider affect the electroweak physics that is done with these detectors.

1. THE DØ AND CDF DETECTORS

The DØ detector[1], shown in Figure 1, consists of three primary systems: a nonmagnetic tracking system, a uranium-liquid argon calorimeter, and a muon spectrometer. The tracking system consists of four detector subsystems: a 3-layer vertex drift chamber, a transition radiation detector, a 4-layer central drift chamber, and two forward drift chambers. The tracking system provides charged particle tracking over the region $|\eta| < 3.2$ in pseudorapidity, where $\eta = -\ln(\tan(\theta/2))$, and θ is the polar angle.

The DØ hermetic, compensating, uranium-liquid argon sampling calorimeter is divided into three parts: a central calorimeter and two end calorimeters. They each consist of an electromagnetic section, a fine hadronic section, and a coarse hadronic section, housed in a steel cryostat. The calorimeter covers the pseudorapidity range $|\eta| < 4.2$ with fine longitudinal segmentation (8 depth segments) and fine transverse segmentation ($\Delta\eta \times \Delta\phi = 0.1 \times 0.1$, where ϕ is the azimuthal angle, and $\Delta\eta \times \Delta\phi = 0.05 \times 0.05$ in the third depth segment of the electromagnetic calorimeter, which is at the electromagnetic shower maximum).

The DØ muon system, used for the identification of muons and determination of their trajectories and momenta, consists of five separate solid-iron toroidal magnets, together with sets of proportional drift tube (PDT) chambers. Typically, one layer of PDT chambers (having four planes) is inside the toroid magnet, and two layers (each with three planes) are located outside of the iron. The muon system covers $|\eta| < 3.3$. The material in the calorimeter and iron toroids combined varies between 13 and 19 interaction lengths.

The CDF detector[2], shown in Figure 2, is a magnetic cylindrical detector with a central barrel region, two end-cap regions closing the barrel, and two far-forward detector regions. It includes a 1.4 T solenoidal magnetic field, charged particle tracking chambers, electromagnetic and hadronic calorimeters, and a muon system. The silicon vertex detector (SVX) consists of four layers of silicon microstrip detectors, providing precise spatial measurements in the r-ϕ plane, and covering $|\eta| < 1.0$. The SVX (with the central tracking chamber) gives a track impact parameter resolution of about $(13 + 40/p_T)$ μm [3], where p_T is the transverse momentum of the track in GeV/c. The vertex tracking chamber ($|\eta| < 3.25$) is a time projection chamber. The central tracking chamber ($|\eta| < 1.1$) is a cylindrical drift chamber containing 84 layers grouped into 9 alternating superlayers of axial and stereo wires.

Outside the CDF solenoid are electromagnetic and hadronic calorimeters ($|\eta| < 1.1$), made of lead or iron absorber sheets interspersed with scintillator, with a segmentation of $\Delta\eta \times \Delta\phi = 0.1 \times 0.26$. A layer of proportional wire chambers is located near shower maximum in the electromagnetic calorimeter to provide a measurement

D∅ Detector

Figure 1. The D∅ detector.
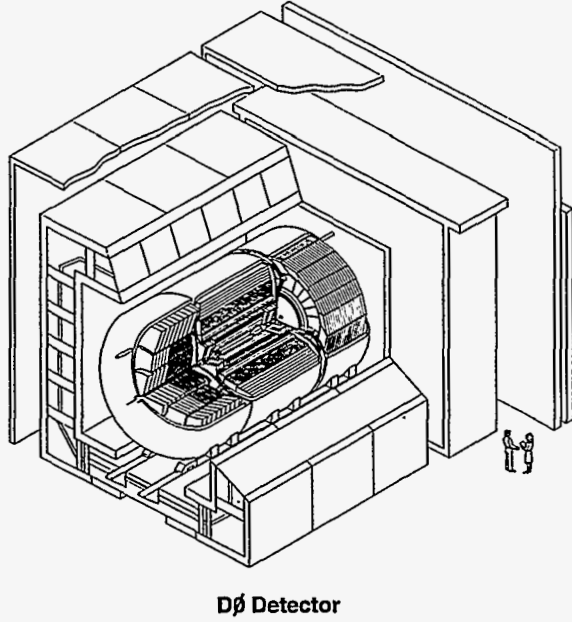

Figure 2. The CDF detector.

of the transverse electromagnetic shower profiles. In the plug end-cap and forward detector regions $(1.1 < |\eta| < 4.2)$, the calorimeters are made of lead or iron absorber sheets sandwiched with conductive plastic proportional tube arrays, with a segmentation of $\Delta\eta \times \Delta\phi = 0.1 \times 0.09$.

The CDF central muon detection system consists of four layers of drift chambers located outside the central hadronic calorimeter, 0.6 m of steel, and four more layers of drift chambers. It covers $|\eta| < 0.6$, and there are 8 interaction lengths of material before the last set of chambers. The region $0.6 < |\eta| < 1.0$ is covered by four free-standing conical arches of drift chambers.

Data taking at the Fermilab Tevatron from 1992–1996, called "Run 1", was divided into three parts:

Run 1A	'92–'93	15–20 pb^{-1} of luminosity
Run 1B	'94–'95	85–90 pb^{-1}
Run 1C	'95–'96	10 pb^{-1}

2. GENERAL DETECTOR REQUIRE-MENTS FOR D∅ AND CDF PHYSICS

Before turning specifically to the electroweak physics that is done with the D∅ and CDF detectors, it is useful to briefly review the general detector requirements necessary for each of the various types of physics done with these detectors. Then in Sections 3,4,5 and 6, we will discuss how the performance aspects of D∅ and CDF affect four specific electroweak physics topics: W and Z Boson Cross Sections, W Boson Mass, W Boson Charge Asymmetry, and Trilinear Gauge Boson Couplings.

2.1. Top Quark Physics

Top quarks produced at the Tevatron decay into W bosons and b quarks. The W bosons then decay into a charged lepton plus neutrino, or into two jets. Thus it is valuable to have a silicon vertex detector for secondary vertex tagging of b-jets, a hermetic calorimeter to reduce QCD and Z+jet backgrounds, a thick absorber in front of the muon system to reduce punch-through for muon tagging, a central magnetic field to help calibrate the calorimeter energy scale and enhance electron identification, good electron, muon and jet identification and efficiency, and fine calorimeter segmentation to reduce errors due to gluon radiation.

2.2. b Quark Physics

To do the best possible job in b-quark physics one needs the ability to reconstruct secondary vertices (with a silicon strip detector or pixel detector) and the ability to reconstruct final states (with a magnetic field). Good inclusive measurements can be done if the detector has good muon and muon+jet triggering (especially for low p_T muons), excellent muon identification (especially at low p_T), large solid angle (eta) coverage for tracking and calorimetry, a thick absorber before the muon chambers to reduce punch-through, and good cosmic ray rejection. Obviously, these considerations are also important for exclusive measurements.

2.3. QCD Physics

One needs large solid angle (eta) coverage (especially for forward jet physics), fine electromagnetic calorimeter depth segmentation (especially for direct photon physics), good electromagnetic and hadronic calorimeter linearity, uniformity, and transverse segmentation, and good jet energy resolution. It is also very useful to have a magnetic field to help calibrate the calorimeter energy scale.

2.4. New Phenomena/Exotics Physics

To search for new particles or new physics beyond the Standard Model, the detector needs to have excellent missing transverse energy resolution (especially in the tail of the distribution), good vertexing in a multiple interaction environment, large solid angle (eta) coverage for leptons, good electromagnetic and hadronic calorimeter hermeticity and energy resolution, and good low energy lepton triggering and identification.

2.5. Electroweak Physics

To do precise measurements in electroweak physics, the detector needs to have good lepton eta coverage, identification and efficiency, and good calorimeter hermeticity, linearity, uniformity, and resolution. It is valuable to have a magnetic field for energy scale calibration, lepton charge determination, and enhanced electron identification. More details on the detector requirements for electroweak physics will be discussed in the rest of this paper.

3. W AND Z BOSON CROSS SECTIONS AND W BOSON WIDTH

The measurement of the production cross sections times leptonic branching ratios ($\sigma \cdot B$) for W and Z bosons allows a determination of the width of the W boson and a comparison of W and Z boson production with QCD predictions. The measurement of the W width can be used to set limits on unexpected decay modes of the W boson (such as W decays into supersymmetric charginos or neutralinos, or heavy quarks).

One determines the leptonic branching ratio of the W boson, $B(W \to l\nu)$, from the ratio of the measured W and Z boson $\sigma \cdot B$ values

$$R \equiv \frac{\sigma_W \cdot B(W \to l\nu)}{\sigma_Z \cdot B(Z \to ll)}, \qquad (1)$$

where $l = e$ or μ, σ_W and σ_Z are the inclusive cross sections for W and Z boson production in $p\bar{p}$ collisions, and $B(Z \to ll)$ is the leptonic branching ratio of the Z boson. One extracts $B(W \to l\nu)$ from the above ratio using a theoretical calculation of σ_W/σ_Z and the precise measurement of $B(Z \to ll)$ from LEP. One then combines $B(W \to l\nu)$ with a theoretical calculation of the W boson leptonic partial width, $\Gamma(W \to l\nu)$, to obtain the W boson total width, $\Gamma(W)$.

In order to measure the W and Z boson cross sections, a detector needs to have excellent identification of high P_T electrons and muons (with high efficiency and low background), large solid angle coverage for electrons and muons, a good missing E_T measurement (as $W \to l\nu$, and the neutrino is inferred from the missing E_T), and an accurate determination of the luminosity.

In particular, for $W \to e\nu$ and $Z \to ee$ one needs fine transverse and longitudinal calorimeter segmentation (for electron identification), excellent calorimeter uniformity over a large range of eta (statistics), excellent calorimeter energy resolution (small error on acceptance), a hermetic calorimeter (for good missing E_T measurement), high tracking efficiency (for electron identification), accurate tracking (for track-calorimeter cluster matching for electron identification), low tracking chamber occupancy (to reduce the fake

rate for backgrounds), accurate vertex determination (for E_T and missing E_T measurement), and efficient counters for the luminosity measurement.

We will now compare the DØ and CDF measurements of the W and Z cross sections and W width in the electron channel:

3.1. Acceptance:

From Table 1 we see that the larger fiducial region for DØ more than makes up for the lower kinematic cuts of CDF. CDF doesn't use forward primary electrons because of poorer tracking and poorer calorimeter segmentation and energy resolution in that region. (CDF does use forward secondary electrons for $Z \rightarrow ee$, and the CDF acceptance then is 10% more than DØ's.) DØ has adequate forward tracking and uniform calorimetry over the whole eta range.

3.2. Efficiency:

The trigger and electron identification efficiency is very similar for both DØ and CDF, and is in the range $70 - 75\%$.

3.3. Background fraction:

	$W \rightarrow e\nu$	$Z \rightarrow ee$
DØ:	$(5.7 \pm 0.5)\%$	$(2.8 \pm 1.4)\%$
CDF:	$(12.3 \pm 1.2)\%$	$(1.6 \pm 0.7)\%$

CDF has a larger W background fraction, possibly due to lower kinematic cuts and poorer missing E_T resolution. The fractional error on the background fraction is about the same for DØ and CDF, but for relatively small background fractions it is the absolute error on the background fraction that is important, and this is smaller for DØ.

3.4. Luminosity error:

The error on the luminosity is 5.4% for DØ and 3.6% for CDF. CDF has a significantly smaller error on the luminosity because they were able to measure the total $p\bar{p}$ cross section (used for luminosity normalization) with their own experiment, while DØ used a world average of CDF and E710 (which disagree, and hence the larger error). The luminosity error is the largest error in the cross section measurement, though it cancels out in the measurement of the ratio of the W and Z cross sections, and thus in the measurement of $\Gamma(W)$.

3.5. Conclusion:

The W cross section and W width results from DØ[4] and CDF[5,6] are shown in Table 2. It appears that in the end DØ and CDF have very similar capabilities for these measurements.

4. W BOSON MASS

In the Standard Model the W boson mass is determined at tree level by three parameters that have been measured to better than 0.01%:

M_Z (mass of the Z boson)

G_μ (Fermi coupling constant)

α (fine structure constant at $q^2 = M_Z^2$)

The W mass is given by:

$$M_W = M_Z cos\theta_W \qquad (2)$$

$$sin^2(2\theta_W) = (4\pi\alpha\sqrt{2})/G_\mu M_Z^2 \qquad (3)$$

At next to leading order in α the W mass is modified by terms corresponding to loop diagrams involving the t and b quarks and the Higgs boson. Thus a sufficiently precise measurement of M_W and M_{top} not only tests the Standard Model, but also constrains the Higgs mass, as is seen, for example, in Figure 3[9].
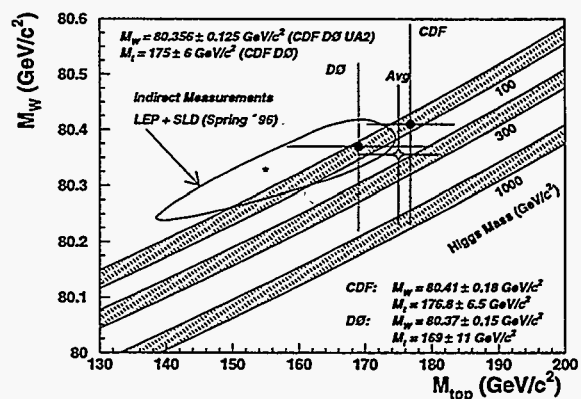

Figure 3. Predictions for M_W as a function of M_{top} in the Standard Model. Preliminary results from DØ and CDF are also shown.

Table 1

$W \to e\nu$ Acceptance for DØ and CDF Cross Section Measurements

	$|\eta|$ Range	E_T cut	Missing E_T cut	$W \to e\nu$ Acceptance
DØ:	<1.1,1.5-2.5	25 GeV	25 GeV	0.460 ± 0.006
CDF:	<1.0	20	20	0.342 ± 0.008

Table 2

W Cross section and $\Gamma(W)$ results for Run 1A

	Luminosity	$\sigma_W B(W \to e\nu)$ ± stat. ± syst. ± lum.	$\Gamma(W)$
DØ:	13 pb^{-1}	2.36 ± 0.02 ± 0.07 ± 0.13 nb	2.044 ± 0.093 GeV
CDF:	21 pb^{-1}	2.49 ± 0.02 ± 0.08 ± 0.09 nb	2.064 ± 0.085 GeV

At the Fermilab Tevatron, W bosons are produced via $p\bar{p} \to W +$ jets, and the W bosons are detected through their leptonic decays: $W \to$ lepton $+ \nu$. One can measure $P_T(\nu)$ from the transverse energy balance, but one can't measure $P_L(\nu)$ because of the unknown amount of energy that went down the beampipe in the forward/backward direction. Thus a true invariant mass cannot be calculated. Instead, one calculates a "transverse mass":

$$M_T^2 = 2E_T^e E_T^\nu (1 - cos\phi^{e\nu}) \qquad (4)$$

The M_T distribution shows a sharp Jacobian peak at the W mass. The W mass is determined from a likelihood fit of the M_T distribution to Monte Carlo generated templates in transverse mass for different W mass values. The E_T^ν measurement depends on the "recoil" momentum of the hadrons. Thus one needs to understand the resolution of, and bias in, both the charged lepton energy measurement and the hadronic recoil measurement in order to correctly model M_T in the Monte Carlo.

In Figure 4 we see a summary[9] of the uncertainties in the DØ and CDF W boson mass measurements. We will concentrate on the Run 1A measurements of the W mass in the electron channel, and compare some aspects of the DØ[7] and CDF[8] measurements. We will discuss the statistical error, and then discuss those uncertainties in the W mass measurement that have the largest difference between the two experiments:

4.1. Statistical error:

The statistical error in the Run 1A W mass measurement in the electron channel is 140 MeV for DØ and 145 MeV for CDF. The number of events in the fitting region is about the same: 5,982 for DØ and 5,718 for CDF (though DØ had an integrated luminosity of 12.8 pb^{-1}, and CDF had 19.7 pb^{-1}).

4.2. Electron angle scale error:

The electron angle scale error in the Run 1A W mass measurement is 50 MeV for DØ and 0 MeV for CDF. DØ has poor vertex determination in multiple interaction events, and poor polar track angle resolution with the tracking system. Thus the electron polar angle, and vertex position, are determined using the calorimeter cluster position and the Z position of the center of gravity of the track in the central tracker. This latter quantity has a bias, and the uncertainty on the correction of the bias gives an uncertainty on M_W of 50 MeV. CDF, with their silicon vertex chamber, has no such problems. Thus it is seen that good tracking is very important, but that one can recover somewhat using a calorimeter with very fine transverse segmentation (and thus good cluster position resolution).

4.3. Energy scale error:

The energy scale error in the Run 1A W mass measurement in the electron channel is 160 MeV for DØ and 120 MeV for CDF.

6

| Summary M_W Uncertainties in MeV |

Source	CDF			DØ	
	e	μ	common	1A	1B
Statistical	145	205	—	140	70
Energy scale	120	50	50	160	80
Angle scale	—	—	—	50	40
e or μ resolution	80	60	—	70	30
p_T^W Model	75	75	65	110	65
pdf's	50	50	50	65	65
QCD/QED corr's	30	30	30	20	20
W-width	20	20	20	20	10
Backgrounds/bias	30	40	5	35	15
Fitting procedure	10	10	—	5	5
Other					70
Total	230	240	100	270	170
Combined		180			150

CDF+DØ (1A)

| $M_W = 80.390 \pm 0.145 \pm 0.065$ GeV/c^2 |

World Average

| $M_W = 80.356 \pm 0.125$ GeV/c^2 |

Figure 4. Uncertainties in the W mass measurement, in MeV. DØ Run 1B values are preliminary.

DØ energy scale error:

Without a magnetic field to calibrate the calorimeter with E/p, the energy scale of the calorimeter is not known precisely enough to use M_W directly from the fit. Thus DØ compares its fitted W mass to its fitted Z mass, and anchors the scale to the precise Z mass as measured at LEP:

$$M_W = [M_W(\text{from } M_T \text{ fit})/$$
$$M_Z(\text{from invariant mass fit})] * M_Z^{\text{LEP}}$$

The normalization and offset of the energy scale were measured with $Z \rightarrow ee, \pi^0 \rightarrow \gamma\gamma$, and $J/\psi \rightarrow ee$ events, resulting in an uncertainty on

Table 3
Uncertainities on M_W, in MeV (Run 1A, electron channel only)

	Stat.	Sys.	E Scale	Total
DØ:	140	165	160	270
CDF:	145	130	120	230

M_W of 160 MeV, of which 150 MeV is due to the statistics of the Z data sample.

CDF energy scale error:

The momentum scale of the central tracker is set by normalizing the measured $J/\psi \rightarrow \mu\mu$ peak to the world-average mass, giving δM_W=50 MeV. The energy scale of the calorimeter is determined from a line-shape comparison of the observed E/p distribution for W$\rightarrow e\nu$ electrons to a detailed MC prediction of this distribution, giving δM_W=110 MeV. Combining these uncertainties gives a total energy scale error of δM_W=120 MeV.

4.4. Conclusion:

It is seen from Table 3 that overall CDF is slightly better than DØ in Run 1A in measuring M_W in the electron channel, due mainly to the central magnetic field (which helps with the energy scale, cross checks, etc).

In addition, the central magnetic field enables CDF to use the muon channel to measure M_W with an uncertainty of 240 MeV[8]. Combined with the electron channel, this results in a total uncertainty for CDF of 180 MeV, which is much better than DØ's 270 MeV. DØ has no central magnetic field, and the momentum resolution of its muon chambers is too poor for a measurement of M_W. With the addition of Run 1B electron data (75 pb^{-1}) DØ's total (preliminary) uncertainty on M_W is 150 MeV[9]. CDF has not yet presented any Run 1B W mass results.

5. W BOSON CHARGE ASYMMETRY

At the Tevatron, W bosons are produced in $p\bar{p}$ collisions primarily by quark-antiquark annihilations:

Table 4
Number of Events Used by DØ and CDF for the Run 1 Asymmetry Measurement.

Channel:	e	μ	μ	$e + \mu$
$|\eta|$:	0-2.4	<1	>1	
DØ:	0	9 K	1 K	10 K
CDF:	73 K	32 K	2 K	107K

$$u + \bar{d} \rightarrow W^+$$
$$\bar{u} + d \rightarrow W^-$$

On average, the $u(\bar{u})$ quarks carry a larger fraction of the momentum of the $p(\bar{p})$ than do the $d(\bar{d})$ quarks, so the $W^+(W^-)$ tends to be boosted in the $p(\bar{p})$ direction. Thus there is a charge asymmetry in the production of W bosons as a function of rapidity. A measurement of this charge asymmetry gives information about the parton distribution functions of the proton (specifically the d/u ratio in the x range of 0.006-0.35). This information about the proton structure is important in the measurement of the W mass, top quark mass, W and Z cross sections, etc.

The W bosons are identified by their $W^\pm \rightarrow l^\pm \nu$ decays. The longitudinal momentum of the ν cannot be measured, so it is actually the charge asymmetry of the decay leptons that is measured. The measured lepton charge asymmetry is a convolution of the charge asymmetry from the W production and the charge asymmetry from the leptonic V-A decay of the W boson.

The DØ Run 1 charge asymmetry results[10] are shown in Figure 5, and the CDF results[11] are shown in Figure 6. One sees that the CDF results are much better than the DØ results. This is because CDF has a factor of 11 more events than DØ for the asymmetry measurement, as seen in Table 4.

DØ can not use electrons for the asymmetry measurement because there is no central magnetic field to determine the charge of the electrons. DØ has a factor of 3.5 fewer muons than CDF, because:

- DØ had a factor of 1.8 smaller effective luminosity due to trigger prescales and main ring blanking. The prescales were neces-
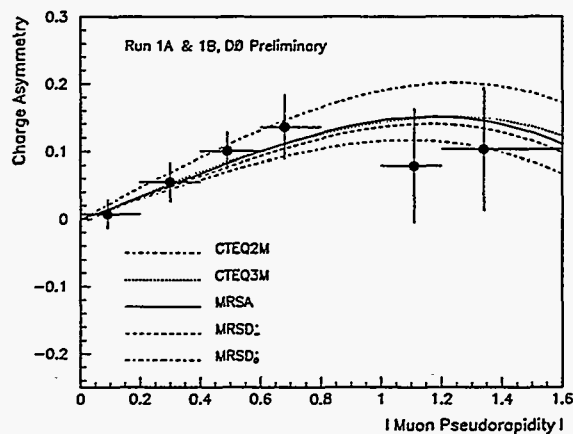

Figure 5. DØ Run 1 Lepton Charge Asymmetry (preliminary).

sary to stay within the small trigger bandwidth. The unscaled trigger rate was large because of the high QCD background due to low momentum muons being mismeasured as high momentum muons and the combinatoric background.

- DØ had a factor of 2.0 lower trigger efficiency because it required tighter trigger cuts (to help reduce the trigger rate) and because its momentum threshold was less sharp (since the muon toroid system has poorer momentum resolution than a central tracker in a magnetic field).

In Run 2 DØ will have comparable statistics to CDF for the asymmetry measurement because:

- DØ will have a solenoidal magnetic field (thus DØ will use the electrons, will have less background for the muon trigger, and will have a sharper muon momentum threshold for the trigger).

- DØ will have increased shielding to reduce combinatorics.

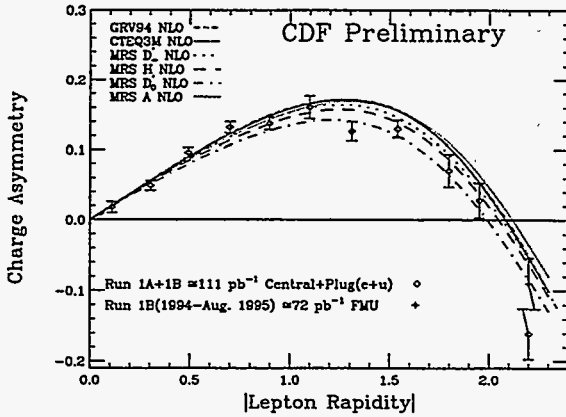- DØ will have a factor of 5 more trigger bandwidth than in Run 1.

Figure 6. CDF Run 1 Lepton Charge Asymmetry (preliminary).

6. TRILINEAR GAUGE BOSON COUPLINGS

A direct consequence of the Standard Model (SM) is the self-interactions of the electroweak gauge bosons (γ, W, Z). The underlying gauge symmetry of the SM yields unique predictions for the strength of these trilinear gauge boson couplings, and any significant deviation from these predictions would be compelling evidence for new physics beyond the SM. A direct measurement of these trilinear couplings ($WW\gamma$, WWZ, $ZZ\gamma$, $Z\gamma\gamma$) is possible by measuring diboson production at the Tevatron.

Non-Standard Model contributions to each trilinear gauge boson interaction can be described by 2 CP-conserving coupling parameters. Nonzero values of these "anomalous" coupling parameters result in a large increase in the corresponding diboson production cross section and a large enhancement of the high P_T tail of the corresponding gauge boson transverse momentum spectrum.

Thus, from the measurement of the diboson cross section (or gauge boson momentum spectrum), one can put limits on the possible deviation from zero of the anomalous coupling param-

eters.

For most of the diboson analyses, DØ and CDF are similar in their abilities to detect the signal, with DØ having a slight advantage. DØ has about a factor of two larger eta coverage, but this is somewhat offset by the higher lepton and photon efficiencies in CDF and the greater integrated luminosity of CDF.

6.1. $W\gamma$ Analyses:

Currently DØ has significantly better limits on anomalous $WW\gamma$ couplings than CDF, as seen in Figure 7[12], but the CDF result is based on a partial Run 1B data set. One sees that the DØ results exclude the $U(1)_{EM-only}$ coupling at the 95% CL, providing direct evidence that the photon couples to more than just the electric charge of the W boson.
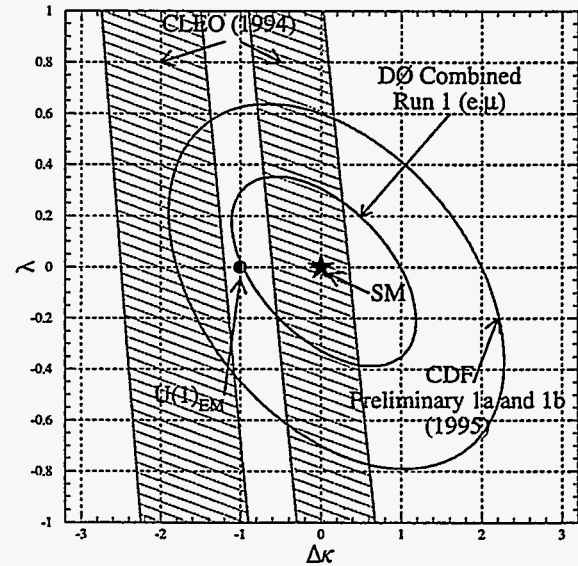

Figure 7. 95% Confidence Limits on Anomalous $WW\gamma$ Couplings, from $W\gamma$ Events.

6.2. WW/WZ Analyses:

Currently CDF has slightly better limits on anomalous WWZ couplings than DØ, as seen

in Figure 8[13], but the DØ results will improve when the same $P_T(W)$ fit that was done for the Run 1A data is done for the Run 1B data. CDF has seen[14] 5 WW events in the dilepton channel, with an expected background of 1.2 ± 0.3 events.
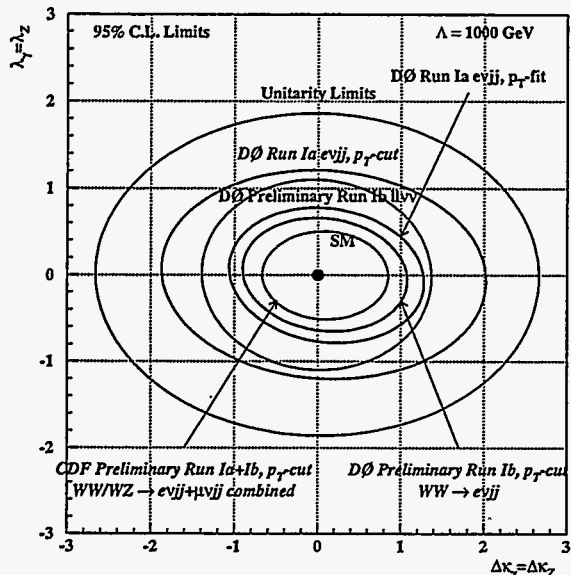

Figure 8. 95% Confidence Limits on Anomalous $WW Z$ Couplings, from WW and WZ Events.

6.3. $Z\gamma$ Analyses:

DØ has significantly better limits on anomalous $ZZ\gamma$ and $Z\gamma\gamma$ couplings than CDF, as seen in Figure 9[15], because of a new measurement by DØ in the $Z(\nu\nu)\gamma$ channel. The sensitivity to anomalous couplings is much higher in the $Z(\nu\nu)\gamma$ channel than in the $Z(l^+l^-)\gamma$ channel due to a higher branching ratio and the absence of diluting radiative Z decay events. But the measurement of $Z(\nu\nu)\gamma$ production is very challenging at a hadron collider because of the extremely high background (due to muon bremsstrahlung, $W \to e\nu$, jet-jet and jet-γ production, etc.). Features of the DØ Detector that enable DØ to do this measurement include:
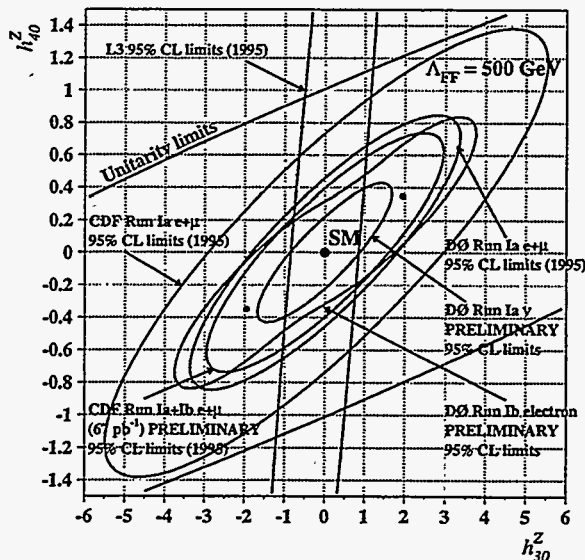

Figure 9. 95% Confidence Limits on Anomalous $ZZ\gamma$ Couplings, from $Z\gamma$ Events.

Hermeticity: The excellent hermeticity of the DØ calorimeter results in a small tail in the missing E_T resolution, and reduces the QCD background.

Hit Counting: Because of the high hit efficiency of the tracking chamber, one can count hit wires to help eliminate background due to $W \to e\nu$, even if the track for the electron is not reconstructed.

Photon "Tracking" in the Calorimeter: Because of the fine longitudinal and transverse segmentation in the DØ electromagnetic calorimeter, one can determine the direction of the photon and determine if it came from the primary vertex, and thus reduce the muon bremsstrahlung background from cosmics and beam halo.

Muon "Tracking" in the Calorimeter: Because one can detect minimum ionizing particles in the DØ calorimeter, one can reduce the muon bremsstrahlung background from cosmic rays and beam halo by searching for a line of minimum ionizing hits in the calorimeter.

7. DØ AND CDF UPGRADED DETECTORS

Run 2 is scheduled for 1999, using the new Main Injector. The expected luminosity is $2*10^{32}$ cm^{-2} sec^{-1}, and the bunch spacing will be 396 ns.

The upgraded DØ Detector[16] for Run 2 will include:

- Completely new tracking system:

  * Silicon vertex detector (barrel + disk system)

  * Scintillating fiber tracker (using high efficiency Visible Light Photon Counters,VLPC's, for photodetectors)

  * Central and forward preshower detector (scintillator strips + VLPC's)

- Central magnetic field (2 Tesla superconducting solenoid)

- New forward muon system (mini-drift tubes + scintillator + shielding)

- New electronics (calorimeter, tracking, muon), trigger, DAQ

The upgraded CDF Detector[17] for Run 2 will include:

- New silicon vertex detector (double-sided barrels)

- New central tracking chamber (open cell drift chamber)

- New forward calorimeters (scintillator tiles)

- Muon system changes (move toroids in, add scintillator, fill gaps)

- New electronics (calorimeter, tracking, muon), trigger, DAQ

8. CONCLUSIONS

DØ and CDF are two large, powerful, multi-purpose detectors with outstanding tracking, calorimeter and muon systems that have done an excellent job in exploiting the Top Quark, b Quark, QCD, New Phenomena/Exotics and Electroweak Physics at the Fermilab Tevatron Collider.

In the Electroweak Physics areas discussed in this paper it is seen that in some areas:

- DØ and CDF have similar performance:

  * W & Z Cross Sections and W Width

- CDF has better performance:

  * W Boson Mass:
  CDF is slightly better than DØ in the electron channel. DØ does not have a measurement in the muon channel (poor $\Delta p/p$).

  * W Boson Charge Asymmetry:
  DØ does not have a competitive measurement because it can not use the electrons (charge not known).

- DØ has better performance:

  * Trilinear Gauge Boson Couplings:
  In most channels DØ is slightly better than CDF. Only DØ has measured the $Z(\nu\nu)\gamma$ channel, and thus has set the tightest limits on anomalous $ZZ\gamma$ and $Z\gamma\gamma$ couplings.

The upgrades of the DØ and CDF detectors will further enhance their capabilities for physics at the Tevatron. The addition of a magnetic field and silicon vertex chamber will open up new physics opportunities for DØ, and the replacement of the plug and forward gas calorimeters with new scintillator-based calorimeters will give CDF uniform calorimetry over all η.

9. ACKNOWLEDGMENTS

REFERENCES

1. S. Abachi *et al.*, Nucl. Instrum. Methods Phys. Res. A338, 185 (1994) and references therein.

2. F. Abe *et al.*, Nucl. Instrum. Methods Phys. Res. **A271**, 387 (1988) and references therein.

3. D. Amidei *et al.*, Nucl. Instrum. Methods Phys. Res. **A350**, 73 (1994).

4. S. Abachi *et al.*, Phys. Rev. Lett. **75**, 1456 (1995).

5. F. Abe *et al.*, Phys. Rev. Lett. **76**, 3070 (1996).

6. F. Abe *et al.*, Phys. Rev. Lett. **73**, 220 (1994); F. Abe *et al.*, Phys. Rev. **D52**, 2624 (1995).

7. S. Abachi *et al.*, Phys. Rev. Lett. **77**, 3309 (1996).

8. F. Abe *et al.*, Phys. Rev. **D52**, 4784 (1995).

9. M. Demarteau, Fermilab-Conf-96/354, Proceedings of the *Meeting of the Division of Particles and Fields*, Minneapolis, August, 1996.

10. A.M. Narayanan, Proceedings of the *Meeting of the Division of Particles and Fields*, Minneapolis, August, 1996.

11. H.S. Budd, Proceedings of the *Meeting of the Division of Particles and Fields*, Minneapolis, August, 1996.

12. S. Abachi *et al.*, Fermilab-Pub-96/434-E (1996), submitted to Phys. Rev. Lett.; The DØ Collaboration, Proceedings of the *28th International Conference on High Energy Physics*, Warsaw, Poland, July, 1996.

13. G. Landsberg, Seminar at Fermilab, http://d0sgi0.fnal.gov/~gll/w&c96/w&c96.html, September 6, 1996 (unpublished).

14. F. Abe *et al.*, Fermilab Pub-96/311-E, submitted to Phys. Rev. Lett.

15. G. Landsberg, Proceedings of the *Meeting of the Division of Particles and Fields*, Minneapolis, August, 1996.

16. The DØ Collaboration, Fermilab-FN-639 (1996).

17. C. Newman-Holmes, Fermilab Conf-96/218-E, Proceedings of the *XI Topical Workshop on $p\bar{p}$ Collider Physics*, Italy, May, 1996.